

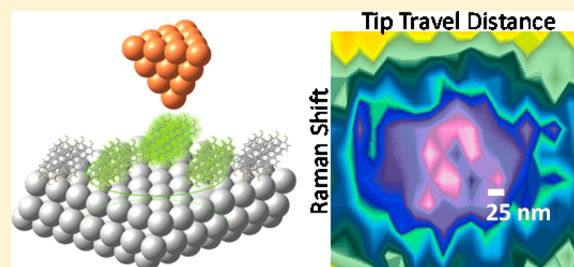
Frequency-Resolved Nanoscale Chemical Imaging of 4,4'-Dimercaptostilbene on Silver

Patrick Z. El-Khoury,*† Tyler W. Ueltschi,‡ Amanda L. Mifflin,‡ Dehong Hu,† and Wayne P. Hess*,†

*Physical Sciences Division, Pacific Northwest National Laboratory, P.O. Box 999, Richland, Washington 99352, United States

‡Department of Chemistry, University of Puget Sound, Tacoma, Washington 98416, United States

ABSTRACT: Nonresonant tip-enhanced Raman (TERS) images of 4,4'-dimercaptostilbene (DMS) molecules adsorbed on silver reveal that different vibrational resonances of the molecules are optimally enhanced at different sites of the metal surface. The recorded images map the interaction between vibrational-mode-dependent polarizability tensors of DMS and enhanced electromagnetic fields at a plasmonic tip–surface nanojunction. TERS images also provide insights into specific molecule–metal interactions. Namely, by virtue of the symmetry (C_{2h}) of the molecular reporter specifically selected for this study, we demonstrate how non-totally symmetric vibrational modes of DMS (b_u modes) map differences in vibronic coupling strength across the metal surface. In effect, each pixel in the recorded TERS images reports on the distinct local environments in which the various probed molecules reside. We illustrate the concept.



INTRODUCTION

Our ability to harness the resonant interaction between optical radiation fields and plasmonic eigenmodes in metal nanostructures has enabled several emerging technologies. The localization of surface plasmons using plasmonic nanostructures and their interaction with molecular polarizabilities have afforded single molecule detection sensitivity^{1–3} in surface-enhanced Raman scattering (SERS)^{4–6} and, more recently, chemical imaging within one molecule⁷ through tip-enhanced Raman scattering (TERS).^{8,9} Single molecule detection sensitivity in Raman spectroscopy can be attained by taking advantage of the localization and enhancement of electric fields at plasmonic nanojunctions where molecules are sited and interrogated. Herein, we closely examine the information content in frequency (8 cm⁻¹ resolution) resolved TERS images (25 nm spatial resolution), recorded by taking advantage of enhanced local electric fields at a plasmonic tip–surface nanojunction. The images are recorded by scanning a 25 nm gold AFM probe through a diffraction-limited laser spot which illuminates a silver substrate coated with 4,4'-dimercaptostilbene (DMS).

Several challenges arise in striving to rigorously interpret enhanced Raman spectra recorded at plasmonic nanojunctions. They mostly stem from our inability to precisely control plasmonic constructs over typical molecular length scales.^{10,11} Recent works have also revealed that when the optical response is nascent from a single scatterer (or a few), the full tensor nature of Raman scattering comes into play.^{7,11–13} Namely, the relative intensities of the observable vibrational states are dictated by the relative orientation of molecules with respect to the enhanced local electric fields. Through TERS point spectra (stationary scanning probe tip), we recently illustrated how subtle temporal variations in TERS intensities can be used to

track molecular orientation at a plasmonic tip–sample nanojunction.¹³ In this work, we build upon our prior analysis and demonstrate how similar effects govern nonresonant TERS imaging experiments which again take advantage of enhanced local electric fields at a plasmonic tip–sample nanojunction. Namely, frequency-resolved TERS images of a silver substrate coated with DMS reveal that different vibrational resonances of the molecule are optimally enhanced at different sites of the metal substrate. The pixelated (25 nm × 8 cm⁻¹) images reconstructed at frequencies corresponding to different vibrational resonances of DMS broadcast intimate details about enhanced local electric field–molecular interactions taking place on much finer scales, which are otherwise only accessible in experiments conducted under ultrahigh vacuum and ultralow temperatures.^{7,14,15} We also exploit the symmetry of DMS (C_{2h} point group) and use its non-totally symmetric vibrational modes (b_u symmetry) to locate regions of the substrate where vibronic coupling is optimal.

METHODS

The samples were prepared using a 0.1 mM solution of 4,4'-dimercaptostilbene (DMS, Sigma-Aldrich) in ethanol (Gold Shield, 200 proof), spin-casted onto ~15 nm Ag films evaporated on a 0.1 mm thick microscope slide by arc-discharge physical vapor deposition (target: Ted Pella Inc., 99.99% purity). The typical surface roughness measured on freshly evaporated silver films indicates a root-mean-square height distribution of ~5 nm. This was followed by rigorously washing the substrate with ethanol and vacuum evaporation to

Received: September 8, 2014

Published: October 22, 2014

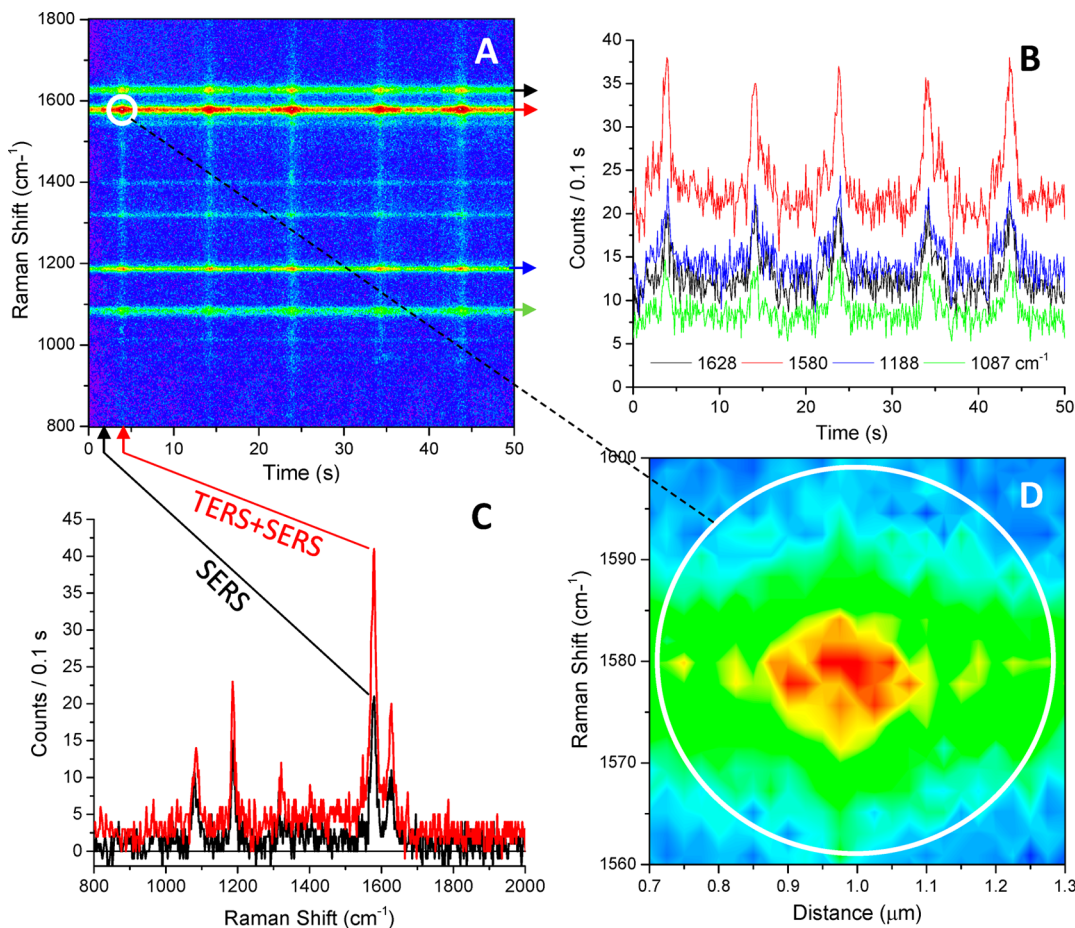


Figure 1. Following laser-tip alignment, the gold AFM probe is scanned back and forth ($\pm 1.25 \mu\text{m}$ in 25 nm increments) through the diffraction-limited laser spot which illuminates the DMS-coated silver substrate. Raman spectra are recorded at every tip position, with an integration time of 0.1 s/spectrum. The overall temporal evolution of enhanced Raman scattering (mixed TERS + SERS) in the $800\text{--}1800\text{ cm}^{-1}$ region is shown in panel A. Panel B shows the time evolution of Raman activity at select vibrational resonances corresponding to strongly allowed (a_g symmetry) Raman transitions in DMS. Notice the rise and decay in intensity for each pass of the AFM tip through the irradiated spot at 4, 14, 24, 34, and 44 s. Panel C shows representative spectra recorded when the tip resides either outside (pure SERS) or toward the center (TERS + SERS) of the laser spot. In panel D, the circled region in panel A is expanded, and the corresponding recorded tip distance is shown on the x -axis.

rid the sample of residual solvent molecules. TERS measurements were conducted under ambient laboratory conditions using an atomic force microscope (Nanoscope IIIa, Veeco Metrology) operating in noncontact mode and mounted on an inverted optical microscope (Axiovert 200, Zeiss). The incident 514 nm continuous wave laser (Innova 300, Coherent) is attenuated to $\sim 45 \mu\text{W}/\mu\text{m}^2$ using a variable neutral density filter wheel, reflected off a dichroic beamsplitter, and focused onto the sample using an oil-immersion objective (1.3 NA, 100 \times). The gold AFM probe (25 nm cone radius) was aligned with the diffraction-limited laser spot by maximizing the nascent molecular signal at $\sim 1580 \text{ cm}^{-1}$. The scattered radiation is collected through the same objective, transmitted through a beamsplitter, and filtered through a long pass filter. The resulting light is detected by a liquid nitrogen cooled charge coupled device coupled to a spectrometer (Holespec f/1.8i, Kaiser Optical System). The effective spectral resolution of our instrument is 8 cm^{-1} .

RESULTS AND DISCUSSION

Following laser-tip alignment, the AFM probe is scanned back and forth ($\pm 1.25 \mu\text{m}$ in 25 nm lateral increments) through the $\sim 250 \text{ nm}$ laser spot which illuminates the DMS-coated silver

substrate. Raman spectra were recorded at every tip position, with an integration time of 0.1 s per spectrum. Figure 1A is a contour plot representation of five Raman images consecutively recorded from five different passes of the AFM probe through the stationary laser spot. Although only five images are shown, the data are representative of some 100 images recorded from different regions of the substrate. The time-dependent scattering signals at select vibrational resonances of the reporter are shown in Figure 1B and can be used to monitor the rise and decay in scattering activity for every pass of the metal AFM probe over the laser-illuminated region of the substrate. When the tip resides outside the laser spot, only SERS is operative. In this case, it is generally accepted that the overall response is dominated by Raman scattering from molecules residing at SERS hotspots within the illuminated region.^{16,17} This accounts for the constant “background” SERS signal. As the tip approaches the laser spot, the molecular signatures are further enhanced. The additional TERS intensity arises from a smaller number of scatterers residing at hotspots, now sustained within the effective near-field scattering area.¹⁸ The TERS/SERS contrast can be discerned by inspecting Figures 1C and 1D. Namely, the constant background signal in Figure 1D corresponds to the average SERS signal when the tip is remote

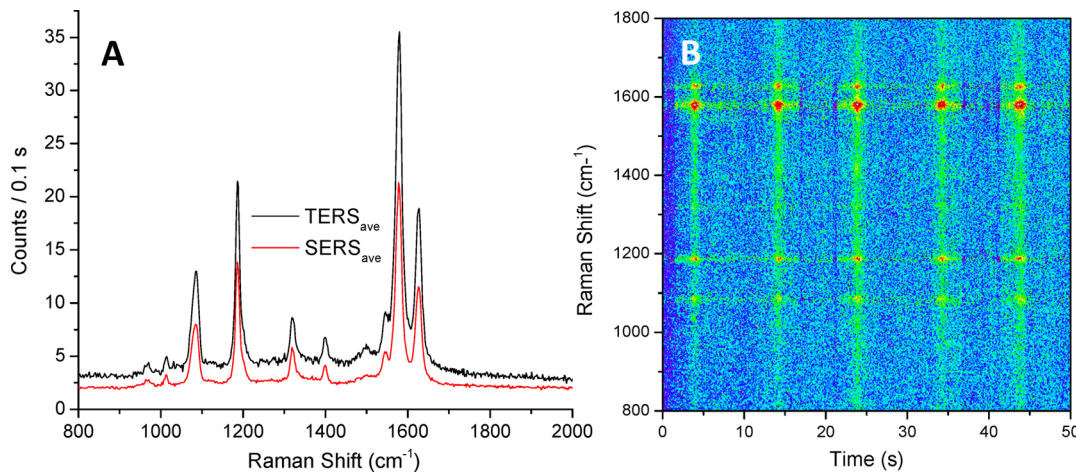


Figure 2. Further analysis of the Raman trajectory shown in Figure 1 allows extracting the pure TERS response and corresponding images for every pass of the AFM tip over the irradiated region of the substrate. This is done by first summing over the spectra recorded in the absence of the tip which yields the pure SERS “background” response. The spatiotemporally averaged SERS spectrum is shown in panel A, along with its TERS + SERS analogue obtained by averaging over the spectra recorded when the tip resides toward the center of the laser spot. Panel B shows the reconstructed pure TERS response, obtained by subtracting the average SERS response from the raw image shown in Figure 1A.

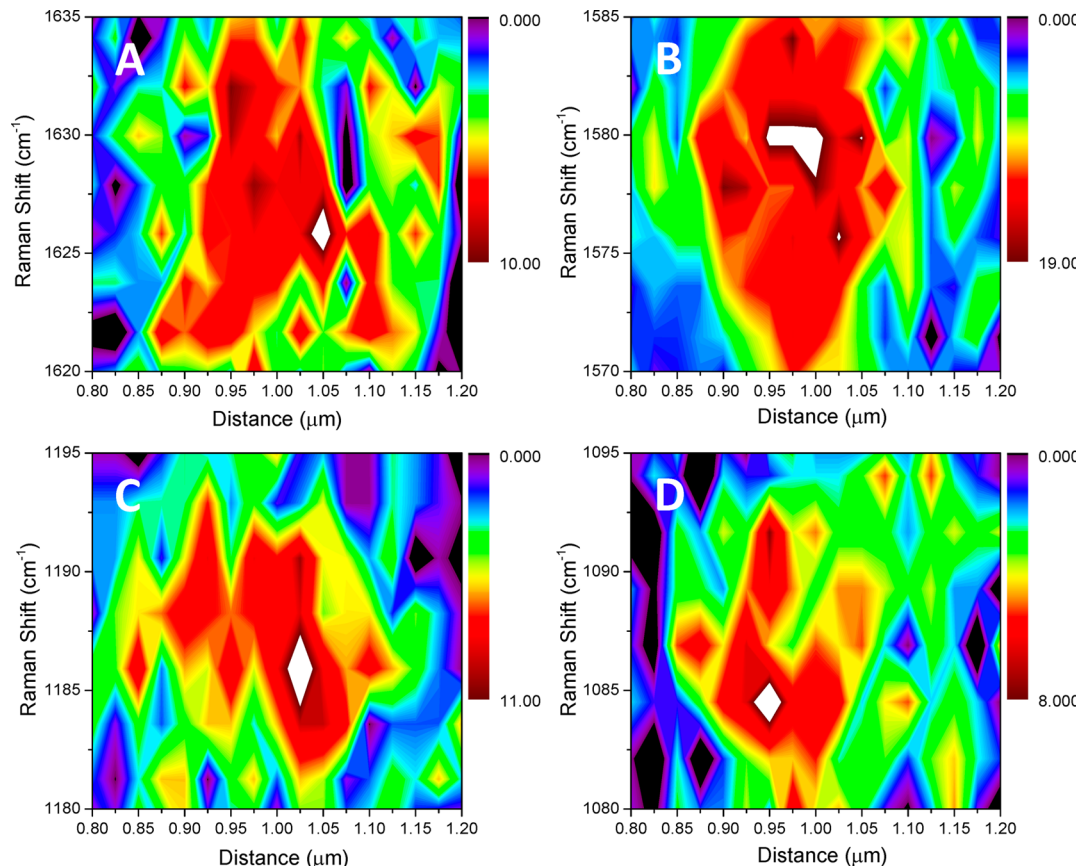


Figure 3. Frequency-resolved TERS (SERS subtracted) images of the laser irradiated region, reconstructed using the four brightest symmetry-allowed Raman vibrational modes (a_g symmetry) of DMS. The representative images are obtained from *the same pass* of the AFM probe through the laser-illuminated region of the substrate. The 2D contours have a color bar starting at white (brightest signals), passing through yellow to black (lowest signals).

from the laser spot, whereas the enhanced response in the $0.975 \pm 0.15 \mu\text{m}$ region is dictated by the interaction of the transient metal tip with the surface, as described below.

Several considerations arise in trying to infer the vector components of the incident and scattered radiation fields at the plasmonic tip–sample nanojunction.^{13,19} Whereas polarization

in the z direction of light propagation (along the tip axis) is required to affect TERS, the polarization of the driving field in our inverted microscope setup is transverse to the tip axis (in the xy plane of the substrate). In principle, this does not allow the incident polarization to efficiently couple into the metal probe, and tip enhancement is not possible. Nevertheless, the

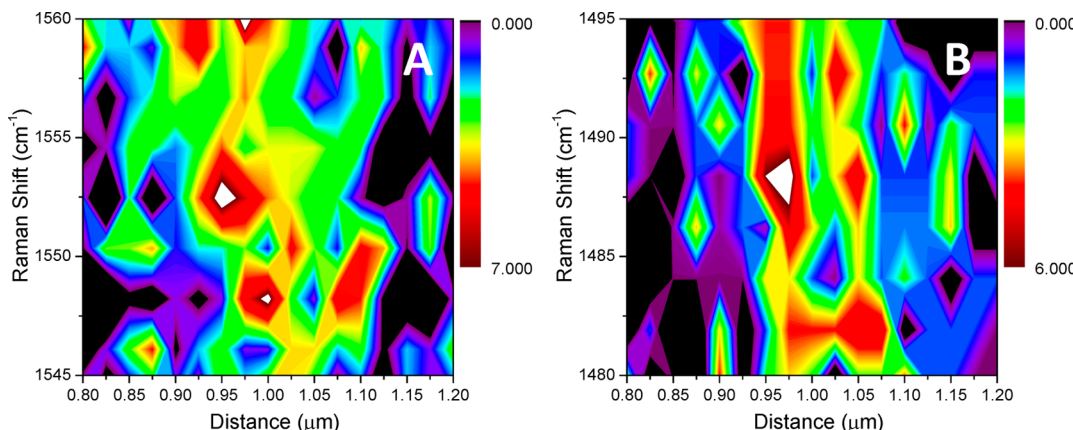


Figure 4. Frequency-resolved TERS (SERS subtracted) images in perspective of two non-totally symmetric Raman modes (b_u symmetry) of DMS. The representative images are obtained from *the same pass* of the AFM probe through the laser-illuminated region of the substrate. The 2D contours have a color bar starting at white (brightest signals), passing through yellow to black (lowest signals).

incident beam is focused onto the sample surface using a high numerical aperture objective (1.3 NA), which partially converts transverse fields to polarization along the tip axis. In an idealized scenario, the corresponding TERS images would effectively trace the spatial distribution of the z component of the electric field. However, this is not what is observed. As previously alluded to, the enhanced TERS response and reconstructed images are biased, as nanometric asperities which convert the incident plane polarized field into radiation in the z direction of light propagation are selectively probed. With the aforementioned considerations in mind, we subtract the average SERS response, measured from the irradiated spot in the absence of the AFM probe, from the total TERS + SERS signal. This yields the pure TERS response and the corresponding images shown in Figure 2B. We use the derived SERS-free images in our ensuing analysis and discussion.

In Figure 3, we zoom into the pure TERS signal recorded in the $0.975 \pm 0.15 \mu\text{m}$ region of the metal substrate, corresponding to *a single pass* (the first pass in Figure 2B) of the AFM probe through the laser-illuminated region. The images are expanded at four frequency shifts corresponding to the strongly Raman allowed totally symmetric vibrational modes of DMS (a_g symmetry). We start by examining the two images reconstructed using the high-frequency vibrational modes centered at 1628 and 1580 cm^{-1} and shown in Figures 3A and 3B. In this case, the signals in the $0.975 \pm 0.15 \mu\text{m}$ region are rather uniform, albeit the signal maxima in the two cases appear at $1.05 \mu\text{m}$ in the 1628 cm^{-1} image and at $0.95-1 \mu\text{m}$ in the 1580 cm^{-1} image. The signal maxima arise from different molecules absorbed at different sites of the silver surface. That optimal TERS activity is frequency/vibrational mode dependent is more evident when the 1188 and 1087 cm^{-1} images are compared (see Figures 3C and 3D). In this case, the brightest TERS signals are separated by $\sim 250 \text{ nm}$, and the distribution of DMS molecules is more localized around the two signal maxima. We stress that all four images shown were recorded from *a single pass* of the AFM tip through the illuminated region of the silver substrate. As such, variations in the experimental setup, e.g., tip drifting, and/or molecular diffusion in/out of the junction cannot account for the above-described observables. Rather, the recorded images broadcast the interaction between the vibrational-mode-dependent molecular polarizability tensors with the distinct local electric

fields interacting with different molecules residing at various sites of the silver substrate.

In the absence of specific molecule–metal interactions^{20,21} which perturb the electronic structure of DMS, and in the dipole coupling limit,¹¹ the scattering tensor which controls TERS activity can be written as¹³

$$S_n^2 = \sum_n |E_s^L \alpha'_n(\Omega) E_i^L|^2 \quad (1)$$

where $E_{i,s}^L$ are the enhanced incident and scattered local radiation fields, α'_n is the molecular polarizability derivative tensor of the n th vibrational eigenstate, and $\Omega = [\alpha, \beta, \gamma]$ are the Euler angles which determine molecular orientation relative to the local electric fields. In this framework, the intensity of the n th vibrational state is dictated by the *relative* orientation of molecules with respect to vector components of $E_{i,s}^L$, herein defined by the interaction of the tip with the nanostructured metal. In principle, the same analysis carried out in ref 13 can be employed to infer the *relative* orientations of DMS molecules with respect to the local electric fields sustained at the different tip positions. We ensure (analysis not shown) that each spectrum recorded in the $0.975 \pm 0.15 \mu\text{m}$ region can be uniquely fitted to distinct relative orientations of DMS with respect to the local electric fields at the different tip positions. That said, we refrain from duplicating our prior analysis¹³ and restrict the present report to the imaging facet of our results. In this regard, notice how the predominant isotropic elements of the molecular polarizability derivative tensor of the brightest 1580 cm^{-1} mode effectively map the laser spot and reveal a rather uniform distribution of DMS molecules in the diffraction-limited spot which illuminates the silver substrate. This is contrasted with the 1188 and 1087 cm^{-1} images plotted in Figures 3C and 3D, where the response is more localized around 1.25 and $0.95 \mu\text{m}$, respectively. Namely, irrespective of the complexity of the enhanced local electric fields, there are always projections of the tensor elements of the predominant 1580 cm^{-1} vibrational mode onto the local fields which effectively leads to its preferential enhancement in the laser-illuminated region of the substrate. Combined with our prior analyses,^{12,13} this observation suggests that normal modes featuring comparable magnitudes of their diagonal and/or off-diagonal polarizability tensor elements serve as better gauges of the local electric field and, hence, result in a more spatially defined TERS response.

The recorded TERS images also provide insights into specific molecule–metal interactions. By virtue of the symmetry of DMS (C_{2h} point group), the observable vibrational Eigenstates can be partitioned into totally symmetric (a_g) and non-totally symmetric (b_u) modes.²² The a_g modes are strongly Raman allowed and derive their intensities through Franck–Condon terms (the A term), whereas the b_u modes are weakly allowed and derive their Raman activity from vibronic coupling terms.^{22,23} Though less intense, especially for DMS in the nonresonant TERS scheme used in this work, images reconstructed using the non-totally symmetric modes of DMS are particularly informative. The images plotted in Figure 4, reconstructed using two vibrational modes with b_u symmetry,²² locate regions of the substrate where vibronic coupling is operative. This interpretation is rather unique, as vibrational modes with b_u symmetry derive the majority of their intensity through vibronic coupling.^{22,23} In this context, the TERS problem is reversed. Rather than using localized electric fields to construct nanoscale chemical maps, we show how unique molecular properties (herein symmetry) and frequency-dependent molecular polarizabilities¹³ can be used to report on the distinct local environments in which different molecules reside.

CONCLUSIONS

We closely examine the information content in TERS images recorded by taking advantage of electric field localization and enhancement at plasmonic tip–sample nanojunctions. We demonstrate how nonresonant TERS images of DMS molecules adsorbed on a metal substrate directly map the interaction between vibrational-mode-dependent polarizability tensors of the molecular reporters and enhanced electromagnetic fields at plasmonic tip–surface nanojunctions. The recorded images additionally provide insights into specific molecule–metal interactions. Herein, we demonstrate that non-totally symmetric vibrational modes of DMS map differences in vibronic coupling strength across the metal surface. In this study, although both the orientation of the probed molecules and the structures of the local electric fields are unknown, we find that their interaction is unique at every tip position. This paves the way for local electric field imaging using TERS, which can be achieved using reporters with well-defined 3D orientations. Such experiments are underway and will be the subject of future reports.

AUTHOR INFORMATION

Corresponding Authors

*E-mail patrick.elkhoury@pnnl.gov; Tel 509-371-6048; Fax 509-371-6145 (P.Z.E.).

*E-mail wayne.hess@pnnl.gov; Tel 509-371-6140; Fax 509-371-6145 (W.P.H.).

Notes

The authors declare no competing financial interest.

ACKNOWLEDGMENTS

P.Z.E. acknowledges support from the Laboratory Directed Research and Development Program through a Linus Pauling Fellowship at Pacific Northwest National Laboratory (PNNL) and an allocation of computing time from the National Science Foundation (TG-CHE130003). W.P.H. acknowledges support from the US Department of Energy (DOE), Office of Science, Office of Basic Energy Sciences, Division of Chemical Sciences,

Geosciences & Biosciences. T.W.U. and A.L.M. were supported in part by the U.S. Department of Energy, Office of Science, Office of Workforce Development for Teachers and Scientists (WDTS) under the Visiting Faculty Program (VFP). This work was performed using EMSL, a national scientific user facility sponsored by DOE's Office of Biological and Environmental Research and located at PNNL. PNNL is a multiprogram national laboratory operated for DOE by Battelle.

REFERENCES

- (1) Nie, S.; Emory, S. R. Probing Single Molecules and Single Nanoparticles by Surface-Enhanced Raman Scattering. *Science* **1997**, *275*, 1102–1106.
- (2) Kneipp, K.; Wang, Y.; Kneipp, H.; Perelman, L.; Itzkan, I.; Dasari, R.; Feld, M. Single Molecule Detection Using Surface-Enhanced Raman Scattering (SERS). *Phys. Rev. Lett.* **1997**, *78*, 1667–1670.
- (3) Le Ru, E.; Etchegoin, P. G. Single-Molecule Surface-Enhanced Raman Spectroscopy. *Annu. Rev. Phys. Chem.* **2012**, *63*, 65–67.
- (4) Fleischmann, M.; Hendra, P. J.; McQuillan, A. J. Raman Spectra of Pyridine Adsorbed at a Silver Electrode. *Chem. Phys. Lett.* **1974**, *26*, 163–166.
- (5) Jeanmaire, D. L.; Van Duyne, R. P. Surface Raman Spectroelectrochemistry: Part I. Heterocyclic, Aromatic, and Aliphatic Amines Adsorbed on the Anodized Silver Electrode. *J. Electroanal. Chem.* **1977**, *84*, 1–20.
- (6) Moskovits, M. Surface Roughness and the Enhanced Intensity of Raman Scattering by Molecules Adsorbed on Metals. *J. Chem. Phys.* **1978**, *69*, 4159–4161.
- (7) Zhang, R.; Zhang, Y.; Dong, Z. C.; Jiang, S.; Zhang, C.; Chen, L. G.; Zhang, L.; Liao, Y.; Aizpurua, J.; Luo, Y.; et al. Chemical Mapping of a Single Molecule by Plasmon-Enhanced Raman Scattering. *Nature* **2013**, *498*, 82–86.
- (8) Steidtner, J.; Pettinger, B. Tip-Enhanced Raman Spectroscopy and Microscopy on Single Dye Molecules with 15 nm Resolution. *Phys. Rev. Lett.* **2008**, *100*, 236101.
- (9) Sonntag, M. D.; Klingsporn, J. M.; Garibay, L. K.; Roberts, J. M.; Dieringer, J. A.; Seideman, T.; Scheidt, K. A.; Jensen, L.; Schatz, G. C.; Van Duyne, R. P. Single-Molecule Tip-Enhanced Raman Spectroscopy. *J. Phys. Chem. C* **2012**, *116*, 478–483.
- (10) Banik, M.; Nag, A.; El-Khoury, P. Z.; Rodriguez-Perez, A.; Guarrotxena, N.; Bazan, G.; Apkarian, V. A. Surface-Enhanced Raman Scattering of a Single Nano-Dumbbell: Dibenzyl-Dithio-Linked Silver Nanospheres. *J. Phys. Chem. C* **2012**, *116*, 10415–10423.
- (11) Banik, M.; El-Khoury, P. Z.; Nag, A.; Rodriguez-Perez, A.; Guarrotxena, N.; Bazan, G.; Apkarian, V. A. Surface-Enhanced Raman Trajectories on a Nano-Dumbbell: Transition from Field to Charge Transfer Plasmons as the Spheres Fuse. *ACS Nano* **2012**, *6*, 10343–10354.
- (12) El-Khoury, P. Z.; Hess, W. P. Raman Scattering from 1,3-Propanedithiol at a Hot Spot: Theory Meets Experiment. *Chem. Phys. Lett.* **2013**, *581*, 57–63.
- (13) El-Khoury, P. Z.; Hu, D.; Hess, W. P. Junction Plasmon-Induced Molecular Reorientation. *J. Phys. Chem. Lett.* **2013**, *4*, 3435–3439.
- (14) Jiang, Y.; Huan, Q.; Fabris, L.; Bazan, G. C.; Ho, W. Submolecular Control, Spectroscopy and Imaging of Bond-Selective Chemistry in Single Functionalized Molecules. *Nat. Chem.* **2013**, *5*, 36–41.
- (15) Lee, J.; Perdue, S. M.; Perez, A. R.; Apkarian, V. A. Vibronic Motion with Joint Angstrom–Femtosecond Resolution Observed Through Fano Progressions Recorded within One Molecule. *ACS Nano* **2014**, *8*, 54–63.
- (16) Fang, Y.; Seong, N.-H.; Dlott, D. D. Measurement of the Distribution of Site Enhancements in Surface-Enhanced Raman Scattering. *Science* **2008**, *321*, 388–391.
- (17) Peppernick, S. J.; Joly, A. G.; Beck, K. M.; Hess, W. P. Plasmonic Field Enhancement of Individual Nanoparticles by Correlated Scanning and Photoemission Electron Microscopy. *J. Chem. Phys.* **2011**, *134*, 034507.

- (18) Pettinger, B.; Schambach, P.; Villagomez, C. J.; Scott, N. Tip-Enhanced Raman Spectroscopy: Near-Fields Acting on a Few Molecules. *Annu. Rev. Phys. Chem.* **2012**, *63*, 379–399.
- (19) Novotny, L.; Hecht, B. *Principles of Nano-Optics*, 1st ed.; Cambridge University Press: New York, 2011.
- (20) El-Khoury, P. Z.; Bylaska, E. J.; Hess, W. P. Time Domain Simulations of Chemical Bonding Effects in Surface-Enhanced Spectroscopy. *J. Chem. Phys.* **2013**, *139*, 174303.
- (21) El-Khoury, P. Z.; Honkala, K.; Hess, W. P. Electronic and Vibrational Properties of Meso-Tetraphenylporphyrin on Silver Substrates. *J. Phys. Chem. A* **2014**, *118*, 8115–8123.
- (22) El-Khoury, P. Z.; Hess, W. P. Vibronic Raman Scattering at the Quantum Limit of Plasmons. *Nano Lett.* **2014**, *14*, 4114–4118.
- (23) Lombardi, J. R.; Birke, R. L. A Unified Approach to Surface-Enhanced Raman Spectroscopy. *J. Phys. Chem. C* **2008**, *112*, 5605–5617.